Available online at www.sciencedirect.com

SciVerse ScienceDirect

Ceramics International 39 (2013) 8411–8419

CERAMICS INTERNATIONAL

www.elsevier.com/locate/ceramint

Characterization of $Ce_{0.8}Sm_{0.2}O_{2-\delta}$-infiltrated $La_{0.8}Ca_{0.2}CoO_{3-\delta}$ cathode for solid oxide fuel cells

Rui-Wei You[a], Jie Ouyang[a], Yen-Pei Fu[a,*], Shao-Hua Hu[b], Kok-Wan Tay[c]

[a]Department of Materials Science and Engineering, National Dong Hwa University, Shou-Feng, Hualien 97401, Taiwan
[b]Department of Environmental Resources Management, Dahan Institute of Technology, Sincheng, Hualien 97145, Taiwan
[c]Department of Electronic Engineering, Wu-Feng University, Minhsiung, Chiayi 62153, Taiwan

Received 13 March 2013; received in revised form 7 April 2013; accepted 7 April 2013
Available online 20 April 2013

Abstract

This work divided into two parts. The first part reports the characteristics of a $La_{0.8}Ca_{0.2}CoO_{3-\delta}$ (LCCO) cathode including its chemical bulk diffusion coefficient (D_{chem}) and chemical surface exchange coefficient (k_{chem}) measured by an electrical conductivity relaxation (ECR) technique. The second part reports two methods to improve the performance of solid oxide fuel cells (SOFCs). One is the use of composite cathode, i.e., mixture of 30 wt% electrolyte and 70 wt% cathode. The other is the use of electrolyte-infiltrated cathode, i.e., the active ionic-conductive electrolyte with nanosize was infiltrated onto a porous cathode surface. In this work, the 0.2 M $Ce_{0.8}Sm_{0.2}O_{1.9}$ (SDC)-infiltrated $La_{0.8}Ca_{0.2}CoO_{3-\delta}$ (LCCO) reveals the maximum peak power density of 305 mW cm^{-2} at operating temperature of 800 °C with a thin film SDC electrolyte (30 μm), a Ni+SDC anode (1 mm) and a SDC-infiltrated LCCO cathode (20 μm). The enhancement in electrochemical performances by using the electrolyte-infiltrated cathode is ascribed to the creation of electrolyte/cathode phase boundaries, which considerably increase the electrochemical sites for oxygen reduction reaction. Therefore, the infiltrated method is a potential way to improve the performance of SOFCs.

Keywords: A. Powders: solid state reaction; C. Diffusion; D. Perovskites; E. Fuel cells

1. Introduction

Recently, solid oxide fuel cells (SOFCs) have attracted a great deal of attention due to the advantages of high electrical efficiency, fuel versatility, low-pollutant emission, etc [1–4]. However, their high operating temperatures above 800 °C limit the application of SOFCs, a lower operating temperature (600–800 °C) is required in the future applications [5]. Cathodes are important components of SOFCs, and developing new cathodes which perform well at the intermediate temperatures (600–800 °C) is a key step in reducing operating temperatures. Potential cathode candidates have normally been based on mixed oxygen ionic and electronic conducting oxides, which have both high ionic and electronic conductivity. The mixed conductivity extends the active oxygen reduction sites from the typical electrolyte–electrode–gas triple-phase boundary to the entire cathode surface, therefore greatly reducing the cathode polarization at low operating temperatures [6]. The development of cathode materials with high eletrocatalytic activity for oxygen reduction reaction at intermediate temperature is great importance and it has received considerable attention during the past decade [7,8]. The cathodic reaction involves the reduction of molecule oxygen to oxygen ion by means of a series of intermediate steps, including gas diffusion, surface adsorption, dissociation, charge transfer and so on [9,10]. Consequently, evaluation the electrocatalytic activity of the cathode towards oxygen reduction at reduced temperature is very important for IT-SOFC. The oxygen reduction activity of an SOFC cathode is closely related to the surface exchange and oxygen bulk diffusion properties. With regard to detailed information of the surface exchange and oxygen bulk diffusion properties will be helpful in understanding the electrochemical properties to perform as a cathode, as well as in providing further guidance on performance optimization [11]. There are several techniques can be applied to determine the surface exchange and bulk diffusion coefficients of a mixed conductor, such as oxygen permeation measurements, coulometric

*Corresponding author. Tel.: +886 3 863 4209; fax: +886 3 863 4200.
E-mail address: d887503@alumni.nthu.edu.tw (Y.-P. Fu).

0272-8842/$ - see front matter © 2013 Elsevier Ltd and Techna Group S.r.l. All rights reserved.
http://dx.doi.org/10.1016/j.ceramint.2013.04.022

titrations, electrochemical impedance spectroscopy, oxygen isotope exchange depth profiling (IEDP) using secondary ion mass spectrometry (SIMS), oxygen isotope exchange using mass spectrometry, and relaxation techniques. The electrical conductivity relaxation (ECR) method has turned out to be a facile way to measure the chemical bulk diffusion coefficient (D_{chem}) and chemical surface exchange coefficient (k_{chem}) of a mixed conductor due to the high sensitivity of electrical conductivity to changes in oxygen concentration or oxygen partial pressure [12–17].

Recently earth-doped cobaltite has attracted much attention as cathode materials for SOFCs due to its mixed-conduction characteristics and its relatively high ionic conductivity. In the present study, $La_{0.8}Ca_{0.2}CoO_{3-\delta}$ (LCCO) was selected as the cathodes to investigate its surface exchange and oxygen bulk diffusion properties. The D_{chem} and k_{chem} of LCCO material at various temperatures and oxygen partial pressures were examined by an ECR method. There are several ways to improve the cathode performance [18–22]. In this work, we chose two ways to improve the cathode performance. One way is the mixture of a high ionic-conductive phase $Ce_{0.8}Sm_{0.2}O_{1.9}$ (SDC) within the cathode. Such a composite cathode can extent the electrochemically active triple phase boundaries (TPBs), where the oxygen reduction reaction (ORR) occurs, and thus improve the electrochemical property. The other way is deposited the active ionic-conductive SDC with nanosize on a porous cathode surface by infiltration. This method could provide a larger number of oxygen reduction reaction sites and improving the electrochemical performance leading relatively low area specific resistances. Finally, the performance of LCCO cathode improved with different ways was investigated systematically.

2. Experimental

2.1. Cathode and electrolyte materials preparation

$La_{0.8}Ca_{0.2}CoO_{3-\delta}$ (LCCO) cathode powder was synthesized by a conventional solid-state reaction synthesis with high purity of La_2O_3, $CaCO_3$, and CoO, powders ($>99\%$) as starting materials. These powders were mixed under ethanol and milled for 12 h using zirconia balls. The ball-milled mixture was dried and grounded into a powder with mortar and then calcined in air at 1000 °C for 4 h. The cathode powders were pelletized with a small amount of PVA as binder. To measure the surface exchange and oxygen bulk diffusion properties of the LCCO cathode, the green bulk with a rectangle shape was applied an uniaxial pressure of 1000 kgf cm^{-2}, then sintered in air at 1200 °C for 4 h with a programmed heating rate of 5 °C min^{-1}. The sintered specimens were made up over 95% of the theoretical density for electrical conductivity measuring. The $Ce_{0.8}Sm_{0.2}O_{1.9}$ (SDC) powder was synthesized by coprecipitation using $Ce(NO_3)_3 \cdot 6H_2O$ and $Sm(NO_3)_3 \cdot 6H_2O$ as the starting materials. The starting materials with stoichiometric ratio were dissolved in distilled water and then added to a solution of ammonia. The mixture solution was adjusted to a pH value in the range of 9.5–10. The resultant precipitate was filtered in a vacuum, and washed three times with water and ethanol, respectively. Then, the coprecipitation powder was calcined in air at 600 °C for 2 h [23].

2.2. Electrical conductivity relaxation (ECR)

The time dependence of the conductivity was measured using the four-probe DC technique, and was recorded by a Keithley 2420 source meter. Measurements were performed on a specimen with a rectangle geometry, having typical size of $5 \times 5 \times 10\ mm^3$ over the temperature range of 500–700 °C at an interval of 50 °C. After each temperature change, the bar was stabilized for at least 30 min. A sudden change in the oxygen partial pressure, from 0.05 to 0.21 atm, was caused by introducing standard gas mixtures of Ar and O_2. The electrical conductivity relaxation curve was plotted as $g(t)$ vs. t, which was fit by a least square method to an analytical solution of Eq. (1); D_{chem} and k_{chem} were the variable fitting parameters [24].

2.3. Symmetrical cell and the single cell fabrication

The cathode paste consisted of cathode powder, solvent, binder, and plasticizer was applied on both sides of SDC electrolyte discs. The screen-printing method was used with the circle patterns of a diameter of 13 mm and a thickness of 1 mm. On one side, the cathode paste was painted as the working electrode (WE) with a surface area of 0.385 cm^2. The Pt reference electrode (RE) was located about 0.3–0.4 cm away from the WE. Such a distance was chosen to avoid measurement errors due to the misalignment of the working and counter electrodes. The Pt counter electrode (CE) was arranged on the other side of the SDC disk. After the cathode material was painted on the electrolyte, it was then sintered at 1000 °C for 4 h in air.

There are three modified LCCO cathodes (working electrodes) were measure their electrochemical properties in this study. The first type (Pure LCCO) was synthesized by the solid-state reaction synthesis method. The second type (Composite LCCO) mixed 70 wt% LCCO cathode with 30 wt% of SDC electrolyte with solid-state reaction synthesis method. The third type (Infiltrated LCCO) was infiltrated SDC electrolyte onto the porous LCCO cathode. For the preparation of the SDC-infiltrated LCCO, aqueous nitrate solution of SDC precursors with 0.2 M was prepared by dissolving proper amount of $Ce(NO_3)_3 \cdot 6H_2O$ and $Sm(NO_3)_3 \cdot 6H_2O$ in water. Ethyl glycol (EG) was also added to the solution as a complex agent to form the correct phase. Ethanol was added into the aqueous solution with a ration of 1:1 to improve the wetting ability on the LCCO backbone. 3 μl of this solution was infiltrated into each side of the porous LCCO cathode using a micro-liter syringe in order to control the amount of loading. After allowing the solution to dry in air, the infiltrated cell was fired at 700 °C for 2 h to obtain the desired SDC nano-sized particles within the LCCO skeleton.

In order to evaluate these cathodes performance in a single cell, the anode-supported fuel cells were prepared. Anode substrates consisting of 58 wt% NiO, 38 wt% SDC and 4 wt% graphite were prepared by a die-pressing process. SDC nanopowder was added onto the pre-pressed green NiO–SDC substrate. And then, the SDC powders and NiO–SDC substrate were co-pressed to form a green bilayer and subsequently co-sintered at 1400 °C for 4 h. The cathode paste was screen-printed onto the SDC electrolyte film supported by NiO–SDC anode and sintered at 1000 °C for 4 h.

2.4. Electrochemical and the single-cell measurements

The symmetrical testing-cell experiments were carried out by using the VoltaLab PGZ301 potentionistat over temperatures ranging from 600 to 800 °C at intervals of 50 °C in a furnace under various oxygen partial pressures. The frequency applied range of the AC impedance measurements ranged from 100 kHz to 0.1 Hz with 10 mV AC signal amplitude. The electrochemical impedance spectroscopy (EIS) fitting analysis was performed with Zview software. Button cells with and without the infiltration of SDC were measured with humidified hydrogen (3 vol% H_2O) as fuel and air as oxidant to evaluate the performance of the fabricated anode-supported solid oxide fuel cells. The current-voltage characteristics of the single cells were measured at the temperature range of 500–800 °C at an intervals of 100 °C.

2.5. Materials characterization

The calcined electrolyte, and cathode were characterized by X-ray powder diffractometer (XRD; Rigaku D/MAX-2500 V), with a scanning rate of 4° min^{-1} and a scanning range of 20–80° using a Cu K_α(1.5418 Å) radiation source. The morphologies of nano-sized SDC-infiltrated LCCO cathode were measured by scanning electron microscopy (SEM; Hitachi 3500H).

3. Result and discussions

3.1. D_{chem} and k_{chem}

The electrode performance is closely related to the intrinsic properties of the electrode material, such as bulk diffusion and surface exchange kinetics properties. In this study, D_{chem} and k_{chem} were measured by an ECR technique, which is based on the principle that a variation in the ambient atmosphere leads to a change in the oxygen vacancy concentration of the mixed ionic and electronic conductor (MIEC). Due to the local electroneutrality requirement, the abrupt change in the oxygen partial pressure of the surrounding atmosphere induces a corresponding change of the charge carrier concentration (oxygen vacancy), which is reflected as a relaxation of the apparent macroscopic electrical conductivity [25]. This relaxation process is accompanied with oxygen exchange at the surface and chemical diffusion in the bulk of the oxide sample. Conductivity relaxation models usually assume small departures from thermal equilibrium and a simple linear model for the surface exchange kinetics [26,27] Fig. 1 shows the typical electrical conductivity relaxation curves of LCCO at various temperatures by a sudden change in the oxygen partial pressure from 0.21 to 0.05 atm.The values for k_{chem} and D_{chem} could be obtained by calculated by fitting the electrical conductivity relaxation curves into Eq. (1).

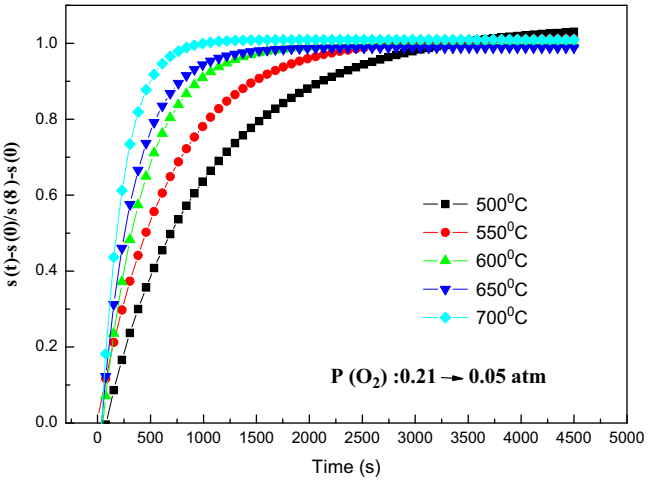

Fig. 1. The electrical conductivity relaxation curve for LCCO at various temperatures after the oxygen pressure suddenly changed from 0.21 to 0.05 atm.

$$\frac{\sigma(t)-\sigma(0)}{\sigma(\infty)-\sigma(0)} = 1-\sum_{n=1}^{\infty}\sum_{m=1}^{\infty}\sum_{p=1}^{\infty} \times \frac{2C_1^2 exp\left(-\alpha_{1n}^2 D_{chem} t/l_1^2\right)}{\alpha_{1n}^2(\alpha_{1n}^2+C_1^2+C_1)} \times \frac{2C_2^2 exp\left(-\alpha_{2m}^2 D_{chem} t/l_2^2\right)}{\alpha_{2m}^2(\alpha_{2m}^2+C_2^2+C_2)} \times \frac{2C_3^2 exp\left(-\alpha_{3p}^2 D_{chem} t/l_3^2\right)}{\alpha_{3p}^2(\alpha_{3p}^2+C_3^2+C_3)} \quad (1)$$

where D_{chem} is the chemical diffusion coefficient, and $\sigma(0)$, $\sigma(t)$, and $\sigma(\infty)$ indicate the initial, time independent and final conductivities, respectively. The coefficients of α_{1n}, α_{2m}, α_{3p} are the nth, mth and pth roots of the transcendental equations:

$$C_1 = \alpha_{1n} tan\alpha_{1n}, \quad C_2 = \alpha_{2m} tan\,\alpha_{2m}, \quad C_3 = \alpha_{3p} tan\alpha_{3p} \quad (2)$$

The parameters of C_1, C_2, and C_3 are defined as:

$$C_1 = \frac{l_1}{L_d}, \quad C_2 = \frac{l_2}{L_d}, \quad C_3 = \frac{l_3}{L_d}, \quad L_d = \frac{D_{chem}}{k_{ex}} \quad (3)$$

where k_{chem} is the surface exchange coefficient in the relaxation process.

The conductivity reached its steady state value faster for the high temperatures than the low temperatures, leading that the values of D_{chem} and k_{chem} at high temperatures were larger than those at low temperatures. The values of D_{chem} for LCCO were 0.25, 1.10, and 2.44×10^{-5} cm^2 s^{-1} at 500, 600, and 700 °C, respectively. With the same trend, k_{chem} were 1.23, 2.51, and 5.23×10^{-3} cm s^{-1} at 500, 600, and 700 °C, respectively. The values regarding D_{chem} and k_{chem} of LCCO cathode in the reduction process were given in Table 1.

The activation energies for D_{chem} and k_{chem} obtained from the slopes of the Arrhenius plots as shown in Fig. 2 were 70

Table 1
k_{chem} and D_{chem} of LCCO at various temperatures from electrical conductivity relaxation curve during the oxygen partial pressure suddenly changed from 0.21 to 0.05 atm.

Temperature (°C)	D_{chem} ($cm^2\ s^{-1}$)	k_{chem} ($cm\ s^{-1}$)
500	2.49×10^{-6}	1.23×10^{-3}
550	5.28×10^{-6}	1.64×10^{-3}
600	1.10×10^{-5}	2.51×10^{-3}
650	1.46×10^{-5}	2.791×10^{-3}
700	2.44×10^{-5}	5.23×10^{-3}

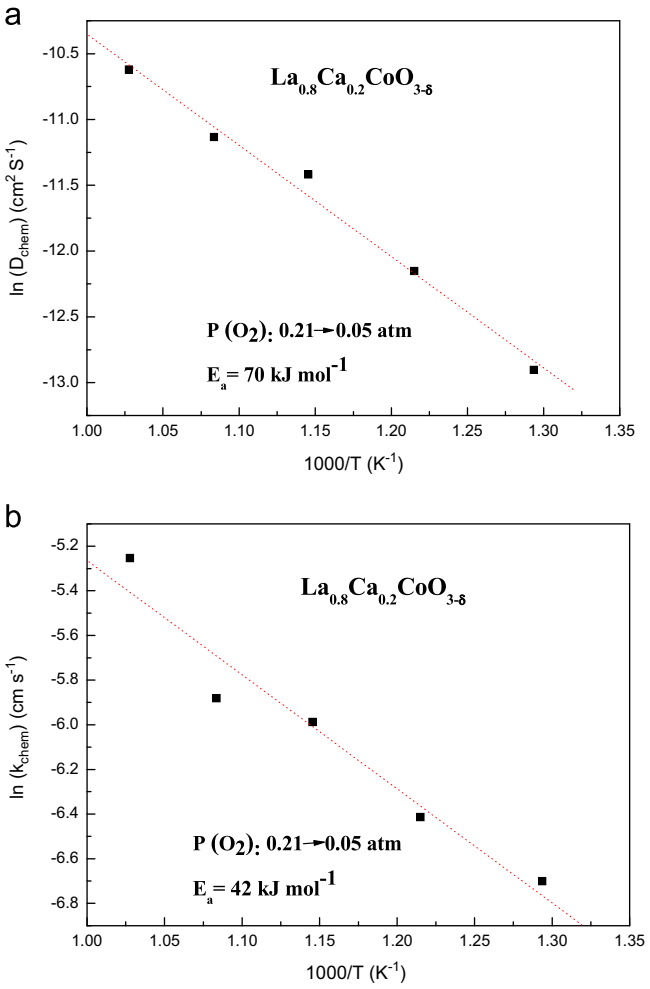

Fig. 2. Arrhenius plots of (a) D_{chem} vs. 1000/T and (b) k_{chem} vs. 1000/T for LCCO cathodes between 500 and 700 °C.

and 42 kJ mol^{-1}, respectively. The equation of D_{chem} as a function of temperature calculated from the Arrhenius plots of D_{chem} vs. 1000/T exhibits as follows:

$$D_{chem} = 2.44 \times 10^{-5} \exp\left(-70 \frac{\text{kJ mol}^{-1}}{RT}\right) (\text{m}^2\ s^{-1}) \quad (4)$$

This equation is applied in the temperature range of 500–700 °C. The activation energy obtained from the Arrhenius plot of D_{chem} may be considered in terms of the enthalpy of mobility of the defects involved in the gas/solid equilibration

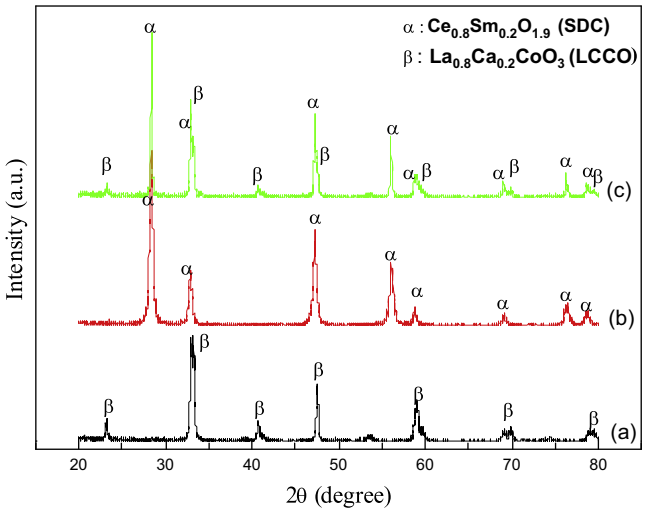

Fig. 3. X-ray diffraction pattern of (a) $La_{0.8}Ca_{0.2}CoO_{3-\delta}$ (LCCO) powder; (b) $Ce_{0.8}Sm_{0.2}O_{1.9}$ (SDC) powder; (c) the powder mixture of 50 wt% LCCO +50 wt% SDC calcined at 1000 °C for 4 h.

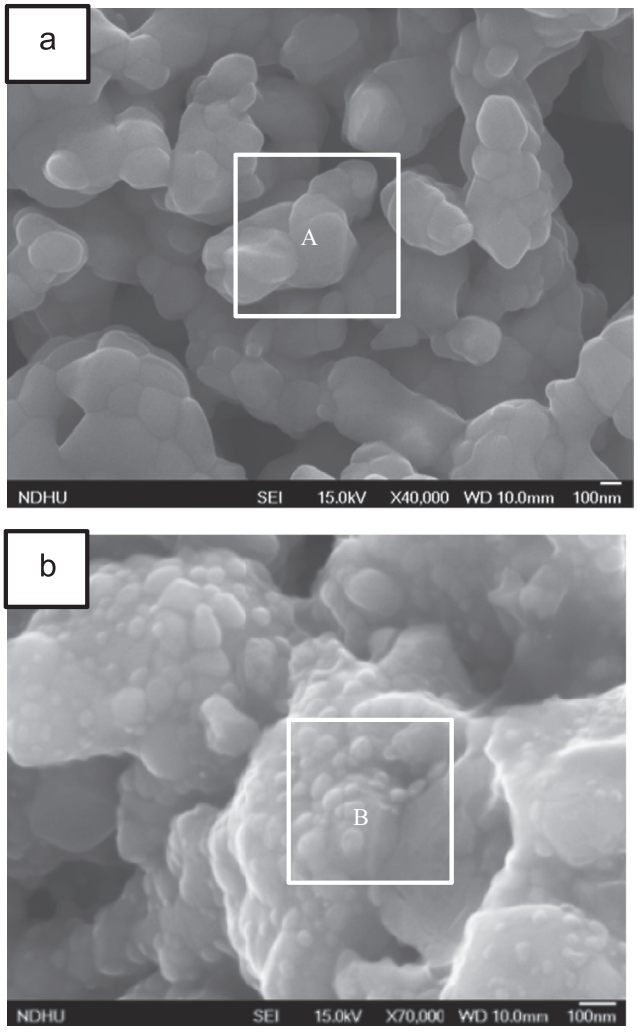

Fig. 4. SEM images of LCCO-based cathodes: (a) pure LCCO; (b) 0.2 M-SDC-infiltrated LCCO.

for the O_2/LCCO system. This may be considered in terms of the effect of oxygen partial pressure and related concentration of defects, and the extent of interactions between the defects and their mobility [28].

3.2. LCCO structure compatibility with SDC electrolyte

The investigation of the solid-state reactions between LCCO and SDC phases is very important for evaluating the chemical stability between cathode and electrolyte during the operating temperature for a long time. As shown in Fig. 3, the XRD patterns of 50 wt% LCCO+50 wt% SDC calcined at 1000 °C for 4 h, LCCO contains a perovskite structure, while SDC contains a cubic fluorite structure, the characteristic peaks of both LCCO and SDC are clear separation for the mixture calcined at 1000 °C. Generally, an electrolyte-infiltrated cathode material sintered at a high temperature with a larger grain size of electrolyte that adhered on cathode skeleton leads to a decrease in the electrode surface area–gas–solid interface (triple phase boundary, TPB), which results in high polarization resistance [29–31]. Meanwhile, due to the high sintering temperature, the cathode materials adhere strongly to the electrolyte surface, resulting in better contact with the electrolyte and better current collection. This represents a trade-off relationship with regard to the sintering temperature to obtain cathode materials with fine microstructure with a lower calcained temperature and strong adhesion to the electrolyte but larger grain-sized electrolyte with a higher calcined temperature. Based on the above-mentioned results, it revealed that no obvious interface reaction appeared for the mixture of LCCO+SDC, indicating the mixture of LCCO+SDC was a chemically stable, when heated up to 1000 °C.

Table 2
The EDS data of LCCO-based cathodes.

Area	Atom (%)					
	Sm L	Ce L	La L	Co K	Ca K	O K
A	–	–	16.84	18.21	1.91	63.04
B	2.17	6.42	34.97	36.19	6.78	13.47

3.3. SEM of LCCO infiltrated with SDC

To improve the cathode performance, the active ionic-conductive SDC nano-sized particles were deposited on a porous LCCO cathode surface by infiltration method. The microstructures of the LCCO cathode infiltrated with and without SDC were observed by SEM, as shown in Fig. 4. To improve the wetting ability between the nitrate solution of SDC precursors and the porous LCCO backbones, a mixture of ethanol and water were used in all specimens. Fig. 4(a) shows the microstructure of pure LCCO cathode, which revealed that LCCO backbone was well sintered and without any tiny SDC particle. The analysis of EDS of area A as listed in Table 2, it revealed that CaO incorporated well with La_2O_3 at A-site of perovskite. After infiltrating with 3 μl of 0.2 M SDC, nanosize SDC particles with tiny grain size in the range of 10–30 nm were introduced to the LCCO backbone as shown in Fig. 4(b). Based on the analysis of EDS, it indicated that SDC nanoparticles indeed deposited on the porous LCCO backbones. Two schematic representations for the way to enhance the area of TPBs are shown in Fig. 5. The first way is to mix the ionic-conductor electrolyte into electronic-conductor cathode as illustrated in Fig. 5(a). The second way is to infiltrate the tiny ionic-conductor electrolyte onto electronic-conductor cathode as shown in Fig. 5(b). Obviously, the infiltration method creates more area of TPBs than the method that mixing the electrolyte into the cathode. The cathode infiltrated with the tiny electrolyte would be expected to reveal lower resistance because of the larger area available for reaction and ion transfer across the interface.

3.4. Interfacial polarization resistances

Fig. 6 shows some typical impedance spectra of the LCCO cathodes improved with various methods which were measured in a symmetric configuration using AC impedance spectroscopy under open-circuit conditions in air from 600–800 °C at the interval of 50 °C. In order to clearly show the difference in the cathode polarization behavior between the Ohmic resistance (R_Ω) and the total cathode polarization resistance (R_P) of the cell, the R_Ω

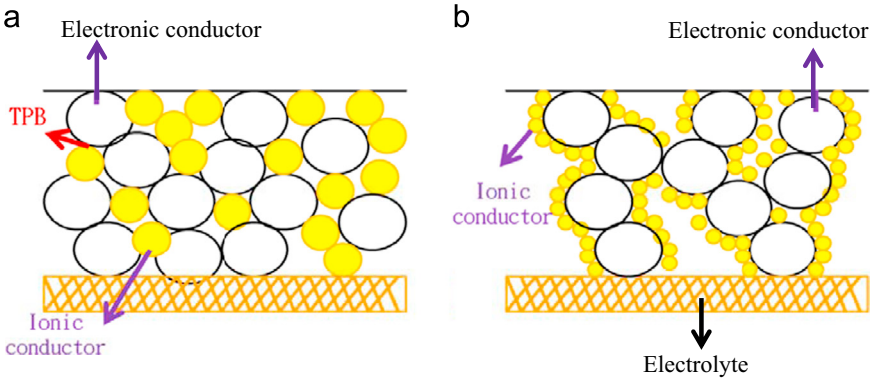

Fig. 5. Schematic representations of (a) mixing ionic-conductor electrolyte into electronic-conductor cathode; (b) infiltrating tiny ionic-conductor electrolyte on electronic-conductor cathode.

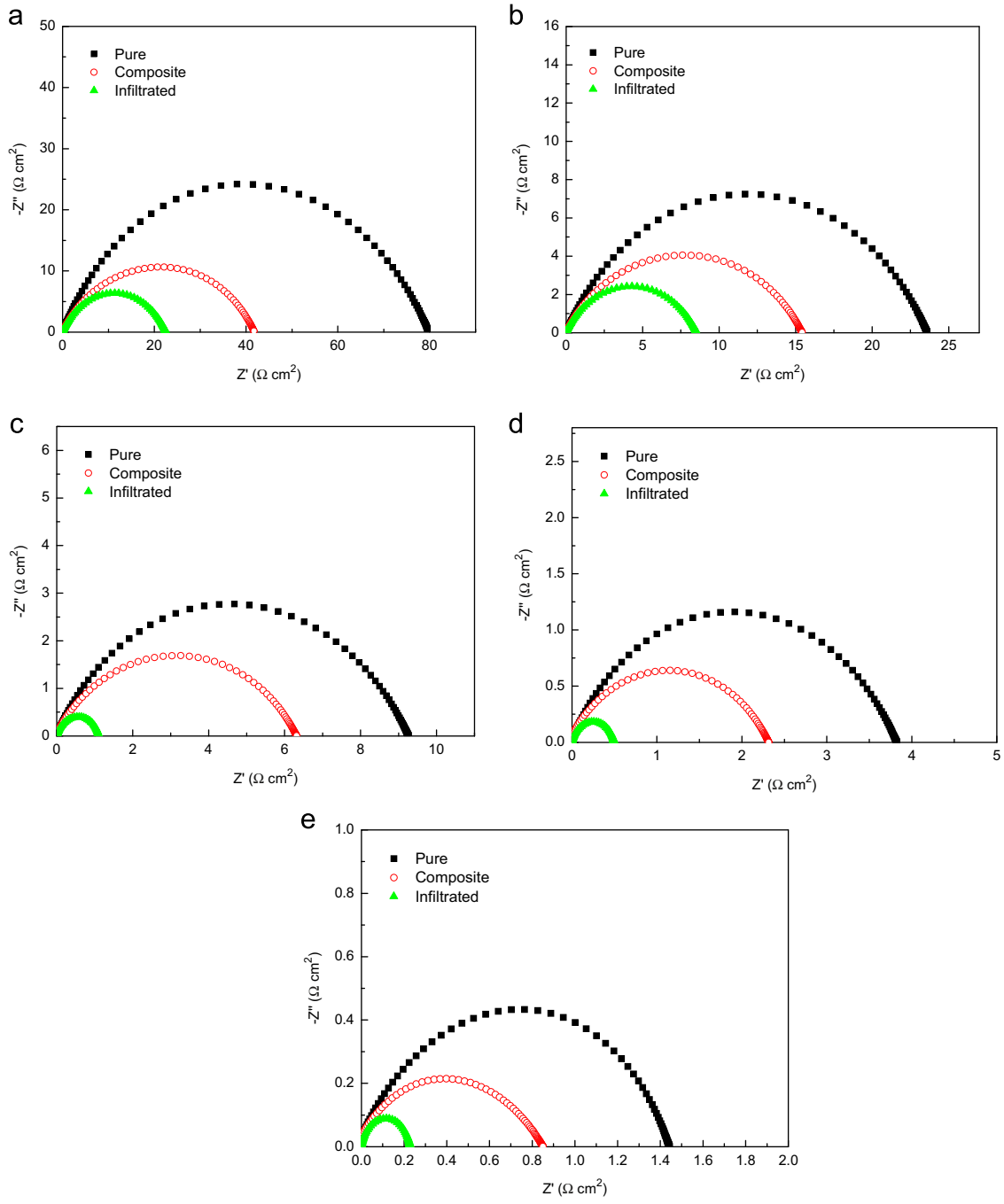

Fig. 6. (a) Impedance spectra for pure, composite, and infiltrated LCCO cathode at various temperatures: (a) 600 °C; (b) 650 °C; (c) 700 °C; (d) 750 °C; and (e) 800 °C.

was eliminated in the impedance plot. The catalytic activity of the LCCO cathodes, as characterized by the R_P, was determined from the size of the impedance loop [32]. The detailed fitting parameters of LCCO cathode improved with different ways were listed in Table 3. The R_p values of pure LCCO cathode were 79.86, 9.28, and 1.46 Ω cm^2 at 600, 700, and 800 °C, respectively. When the SDC mixed into the LCCO cathode, the R_p values were reduced to 41.87, 6.36, and 0.88 Ω cm^2 at 600, 700, and 800 °C, respectively. When the SDC infiltrated on the LCCO cathode, the R_p values

Table 3
Results of the fitting parameters of LCCO cathode improved with different methods at various temperatures.

Sample	R_P (Ω cm^2)				
	600 °C	650 °C	700 °C	750 °C	800 °C
LCCO (Pure)	79.86	23.62	9.28	3.84	1.46
LCCO (Composite)	41.87	15.47	6.36	2.36	0.88
LCCO (Infiltrated)	22.32	8.56	1.11	0.50	0.23

were further reduced to 22.32, 1.11, and 0.23 Ω cm^2 at 600, 700, and 800 °C, respectively. After infiltration, the impedance spectrum shape seemingly changed that both high- and low-frequency arcs were obviously reduced. It indicated that both electrochemical processes (i.e. the electrochemical reactions at the electrode–electrolyte interface and adsorption–desorption of oxygen, oxygen diffusion at the gas-cathode surface interface.) were simultaneously improved by active SDC nono-sized particles deposited on LCCO cathode backbone. The dramatic decrease in R_p was mainly attributed to the creation of SDC/LCCO phase boundaries. The newly formed SDC deposited on the LCCO cathode with highly porous skeleton would allow gas-phase molecules to easily diffuse to the SDC/LCCO boundaries, which considerably increased the electrochemical sites for oxygen reduction reaction (ORR) [33]. The ORR sites were not only at the real LCCO cathode surface area simultaneously exposed to electrolyte and air, but also at these newly formed SDC nano-sized particles deposited on LCCO porous skeleton. Apparently, the area of TPBs greatly affects the electrochemical performance of cathode.

3.5. Single cell performance

To evaluate the LCCO cathode improved with different ways, an anode-supported single fuel cell with a thin film SDC electrolyte (30 μm), a Ni+SDC anode (1 mm) and a LCCO cathode (20 μm) was fabricated. The performance (including *I–V* curve and *I–P* curve under different operating temperatures) of the LCCO cathode improved with different ways as shown in Fig. 7. Generally, the open-circuit voltage (OCV) of an ideal cell should be close to its theoretic value of 1.1 V, and slightly influenced by the operating condition. In this study, the values of practical OCV were lower than its theoretical value, this might be ascribed to the following reasons. First, the SDC electrolyte possessed minor electronic conductivity, a slight electron cross flow (current leakage) might occur through the electrolyte. Second, the electrolyte membrane might be not dense, the fuel/oxidant cross flow could take place. The higher the current leakage exists, the lower the cell OCV will be. As shown in Fig. 7(b), the current–voltage curves and the corresponding power densities for cells were measured at 600 °C. The peak power densities of 106 and 151 mW cm^{-2} were achieved for composite, and infiltrated LCCO. When the operating temperatures were increased to 700 °C, the peak power densities were increased to 196 and 259 mW cm^{-2} for composite, and infiltrated LCCO as shown in Fig. 7(c). As the operating temperature was increased to 800 °C, the peak power densities were further increased to 235 and 305 mW cm^{-2} for composite, and infiltrated LCCO as shown in Fig. 7(d). The LCCO cathode improved with various ways, the levels in improvement of electrochemical properties performance of the anode-supported single cells are different, and the peak power densities at the temperature range of 500–800 °C were shown in Table 4. Apparently, the LCCO cathode improved with infiltrated method exhibited the best

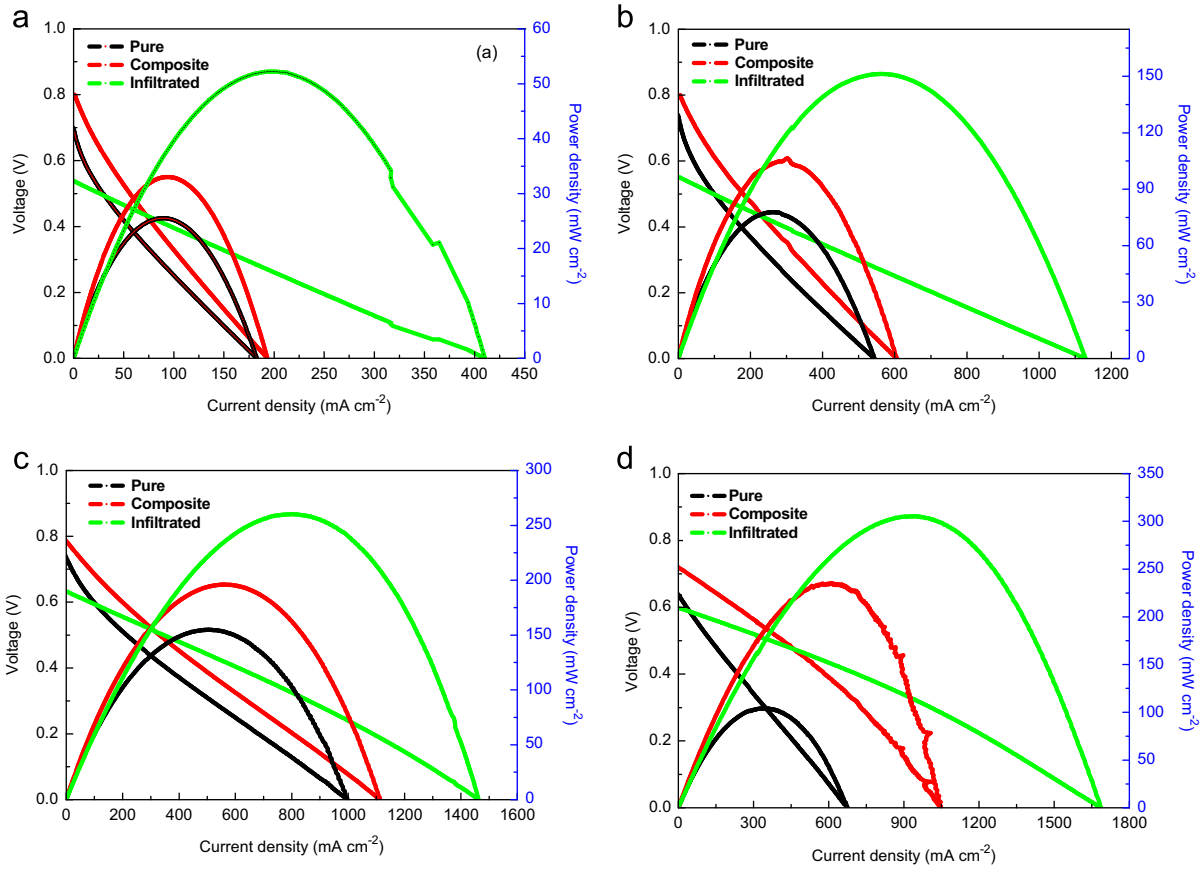

Fig. 7. The *I–V* and *I–P* curves for SOFCs with a LCCO cathode improved with different methods at various temperatures (a) 500 °C; (b) 600 °C; (c) 700 °C; and (d) 800 °C.

Table 4
The peak power densities in the temperature range of 500–800 °C of the anode-supported single cells for LCCO cathode improved with different ways.

Sample	The peak power density (mW cm^{-2})			
	500 °C	600 °C	700 °C	800 °C
LCCO (Pure)	25	78	155	104
LCCO (Composite)	33	106	196	235
LCCO (Infiltrated)	52	151	259	305

performance, i.e., 0.2 M SDC-infiltrated LCCO reveals the maximum peak power density of 305 mW cm^{-2} at operating temperature of 800 °C. However, the values of practical OCV were much lower than theoretical value. If we can fabricate a dense electrolyte membrane in the future, the value of OCV might reach the theoretical. Then, the values of power density might enhance greatly. The infiltration technique was performed to improve the electrochemical properties of cathode. The newly formed electrolyte of SDC nano-sized powders deposited on the LCCO cathode would allow gas-phase molecules to easily diffuse to the SDC/LCCO boundaries where the sites took place ORR.

4. Conclusions

The oxygen reduction activity of an SOFC cathode is closely related to the surface exchange and oxygen bulk diffusion properties. The knowledge regarding D_{chem}, and k_{chem} of mixed conductors would be useful for practical applications. Through the electrical conductivity relaxation test, the values of D_{chem} of LCCO were from 2.46×10^{-6} cm^2 s^{-1} for 500 °C to 2.44×10^{-5} cm^2 s^{-1} for 700 °C. With the same tendency, the values of k_{chem} were from 1.23×10^{-3} cm s^{-1} for 500 °C to 5.23×10^{-3} cm s^{-1} for 700 °C. The activation energies for D_{chem} and k_{chem} were 70 and 42 kJ mol^{-1}, respectively. To improve the electrochemical properties of cathode, LCCO cathode improved with two ways. One is the use of composite cathode, the other is the use of electrolyte-infiltrated cathode. Based on the experimental results, it is revealed that the LCCO cathode infiltrated with 3 μL of 0.2 M SDC with optimum peak power density of anode-supported SOFC single cell was 305 mW cm^{-2} at 800 °C. This behavior suggested that the infiltration of electrolyte nano-sized powder deposited on porous skeleton cathode significantly improved the electrochemical properties of cathode. The obvious increase in electrochemical performances was mainly attributed to the creation of electrolyte/cathode phase boundaries. The newly formed electrolyte nano-sized particles deposited on the porous skeleton cathode would allow gas-phase molecules to easily diffuse to the electrolyte/cathode boundaries, increasing the electrochemical sites for oxygen reduction reaction.

Acknowledgments

The authors would like to thank the National Science Council of Taiwan for financially supporting this research under Contract no. NSC 101–2113-M-259-004.

References

[1] X. Ding, X. Kong, H. Wu, Y. Zhu, J. Tang, Y. Zhong, $SmBa_{0.5}Sr_{0.5}Cu_2O_{5+\delta}$ and $SmBa_{0.5}Sr_{0.5}CuFeO_{5+\delta}$ layered perovskite oxides as cathodes for IT-SOFCs, International Journal of Hydrogen Energy 37 (2012) 2546–2551.
[2] Y.H. Chena, Y.J. Wei, H.H. Zhong, J.F. Gao, X.Q. Liu, G.Y. Meng, Synthesis and electrical properties of $Ln_{0.6}Ca_{0.4}FeO_{3-\delta}$ (Ln=Pr, Nd, Sm) as cathode materials for IT-SOFC, Ceramics International 33 (2007) 1237–1241.
[3] J.H. Kim, H. Kim, $Ce_{0.9}Gd_{0.1}O_{1.95}$ supported $La_{0.6}Sr_{0.4}Co_{0.2}Fe_{0.8}O_{3-\delta}$ cathodes for solid oxide fuel cells, Ceramics International 38 (2012) 4669–4675.
[4] S.C. Singhal, Solid oxide fuel cells for stationary, mobile, and military applications, Solid State Ionics 152 (2002) 405–410.
[5] H. Moon, S.D. Kim, S.H. Hyun, S.H. Kim, Development of IT-SOFC unit cells with anode-supported thin electrolytes via tape casting and co-firing, International Journal of Hydrogen Energy 33 (2008) 1758–1768.
[6] W. Zhou, Z. Shao, R. Ran, P. Zeng, H. Gu, W. Jin, N. Xu, $Ba_{0.5}Sr_{0.5}Co_{0.8}Fe_{0.2}O_{3-\delta}$+$LaCoO_3$ composite cathode for $Sm_{0.2}Ce_{0.8}O_{1.9}$-electrolyte based intermediate-temperature solid-oxide fuel cells, Journal of Power Sources 168 (2007) 330–337.
[7] Z.P. Shao, S.M. Haile, A high-performance cathode for the next generation of solid-oxide fuel cells, Nature 431 (2004) 170–173.
[8] W. Zhou, Z.P. Shao, R. Ran, W.Q. Jin, N.P. Xu, A novel efficient oxide electrode for electrocatalytic oxygen reduction at 400–600 °C, Chemical Communications 44 (2008) 5791–5793.
[9] B.W. Liu, Y. Zhang, L.M. Zhang, Oxygen reduction mechanism at $Ba_{0.5}S_{r0.5}Co_{0.8}Fe_{0.2}O_{3-\delta}$cathode for solid oxide fuel cell, International Journal of Hydrogen Energy 34 (2009) 1008–1014.
[10] X.J. Chen, S.H. Chan, K.A. Khor, Simulation of a composite cathode in solid oxide fuel cells, Electrochim Acta 41 (2004) 1851–1861.
[11] D. Chen, Z. Shao, Surface exchange and bulk diffusion properties of $Ba_{0.5}Sr_{0.5}Co_{0.8}Fe_{0.2}O_{3-\delta}$ mixed conductor, International Journal of Hydrogen Energy 36 (2011) 6948–6956.
[12] E. Bucher, A. Egger, P. Ried, W. Sitte, P. Holtappels, Oxygen nonstoichiometry and exchange kinetics of $Ba_{0.5}Sr_{0.5}Co_{0.8}Fe_{0.2}O_{3-\delta}$, Solid State Ionics 179 (2008) 1032–1035.
[13] X. Chen, S. Wang, Y.L. Yang, L. Smith, N.J. Wu, B.I. Kim, S.S. Perry, A. J. Jacobson, A. Ignatiev, Electrical conductivity relaxation studies of an epitaxial $La_{0.5}Sr_{0.5}CoO_{3-\delta}$ thin film, Solid State Ionics 146 (2002) 405–413.
[14] A. Zomorrodian, H. Salamati, Z.G. Lu, X. Chen, N.J. Wu, A. Ignatiev, Electrical conductivity of epitaxial $La_{0.6}Sr_{0.4}Co_{0.2}Fe_{0.8}O_{3-\delta}$ thin films grown by pulsed laser deposition, International Journal of Hydrogen Energy 35 (2010) 12443–12448.
[15] I. Yasuda, T. Hikita, Precise determination of the chemical diffusion coefficient of calcium-doped lanthanum chromites by means of electrical conductivity relaxation, Journal of the Electrochemical Society 141 (1994) 1268–1273.
[16] I. Yasuda, M. Hishinuma, Electrical conductivity and chemical diffusion coefficient of Sr-doped lanthanum chromites, Solid State Ionics 80 (1995) 141–150.
[17] I. Yasuda, M. Hishinuma, Electrical conductivity and chemical diffusion coefficient of strontium-doped lanthanum manganites, Journal of Solid State Chemistry 123 (1996) 382–390.
[18] B. Wei, Z. Lu, T. Wei, D. Jia, X. Huang, Y. Zhang, J. Miao, W. Su, Nanosized $Ce_{0.8}Sm_{0.2}O_{1.9}$ infiltrated $GdBaCo_2O_{5+\delta}$ cathodes for intermediate-temperature solid state oxide fuel cells, International Journal of Hydrogen Energy 36 (2011) 6151–6159.
[19] Y.Y. Huang, K. Ahn, J.M. Vohs, R.J. Gorte, Characterization of Sr-doped $LaCoO_3$–YSZ composites prepared by impregnation methods, Journal of the Electrochemical Society 151 (2004) A1592–1597.
[20] T.Z. Sholklapper, C. Lu, C.P. Jacobson, S.J. Visco, L.C. De Jonghe, LSM-infiltrated solid oxide fuel cell cathodes, Electrochemical and Solid-State Letters 9 (2006) A376–378.
[21] M. Shah, S.A. Barnett, Solid oxide fuel cell cathodes by infiltration of $La_{0.6}Sr_{0.4}Co_{0.2}Fe_{0.8}O_{3-\delta}$ into Gd-Doped Ceria, Solid State Ionics 179 (2008) 2059–2064.

[22] J.M. Vohs, R.J. Gorte, High-performance SOFC cathodes prepared by infiltration, Advanced Materials 21 (2009) 943–956.
[23] Y.P. Fu, S.B. Wen, C.H. Lu, Preparation and characterization of samaria-doped ceria electrolyte materials for solid oxide fuel cells, Journal of the American Ceramic Society 91 (2008) 127–131.
[24] C. Huang, D. Chen, Y. Lin, R. Ran, Z. Shao, Evaluation of $Ba_{0.6}Sr_{0.4}Co_{0.9}Nb_{0.1}O_{3-\delta}$ mixed conductor as a cathode for intermediate-temperature oxygen-ionic solid-oxide fuel cells, Journal of Power Sources 195 (2010) 5176–5184.
[25] H. Dunwald, C. Wagner, Measurement of diffusion rate in the process of dissolving gases in solid phases, Zeitschrift für Physikalische Chemie B 24 (1934) 53–58.
[26] I. Yasuda, H. Hikita, Precise determination of the chemical diffusion coefficient of calcium-doped lanthanum chromites by means of electrical conductivity relaxation, Journal of the Electrochemical Society 141 (1994) 1268–1273.
[27] J.E. Elshof, M.H.R. Lankhorst, H.J.M. Bouwmeester, Oxygen exchange and diffusion coefficients of strontium-doped lanthanum ferrites by electrical conductivity relaxation, Journal of the Electrochemical Society 144 (1997) 1060–1067.
[28] T. Bak, J. Nowotny, C.C. Sorrel, Chemical diffusion in calcium titanate, Journal of Physics and Chemistry of Solid 65 (2004) 1229–1241.
[29] H.J. Hwang, J.W. Moon, J. Moon, M. Awano, Removal of nitric oxide (NO) by perovskite-type composite catalytic thick film, $La_{0.6}Sr_{0.4}Co_{0.2}Fe_{0.8}O_{3-\delta}$ and Gadolinia-Doped Ceria Electrolyte, $Gd_{0.2}Ce_{0.8}O_{2-\delta}$, Journal of the American Ceramic Society 88 (2005) 79–84.
[30] H.J. Hwang, J.W. Moon, S. Lee, E.A. Lee, Electrochemical performance of LSCF-based composite cathodes for intermediate temperature SOFCs, Journal of Power Sources 145 (2005) 243–248.
[31] Y.P. Fu, C.H. Li, S.H. Hu, Comparison of the electrochemical properties of infiltrated and functionally gradient $Sm_{0.5}Sr_{0.5}CoO_{3-\delta}$-$Ce_{0.8}Sm_{0.2}O_{1.9}$ composite cathodes for solid oxide fuel cells, Journal of the Electrochemical Society 159 (2012) B629–634.
[32] L. Nie, M. Liu, Y. Zhang, M. Liu, $La_{0.6}Sr_{0.4}Co_{0.2}Fe_{0.8}O_{3-\delta}$ cathodes infiltrated with samarium-doped cerium oxide for solid oxide fuel cells, Journal of Power Sources 195 (2010) 4704–4748.
[33] S.P. Jiang, Nanoscale and nano-structured electrodes of solid oxide fuel cells by infiltration: Advances and challenges, International Journal of Hydrogen Energy 37 (2012) 449–470.